NATIONAL AERONAUTICS AND SPACE ADMINISTRATION

Technical Report No. 32-1037

The Design and Testing of an Inflated Sphere Impact Limiter

R. G. Ross, Jr.

W. E. Layman

GPO PRICE $ _____

CFSTI PRICE(S) $ _____

Hard copy (HC) 3.00

Microfiche (MF) .65

ff 653 July 65

N67 14906

(ACCESSION NUMBER) | (THRU)

35 | 1

(PAGES) | (CODE)

CR-81030 | 32

(NASA CR OR TMX OR AD NUMBER) | (CATEGORY)

FACILITY FORM 602

JET PROPULSION LABORATORY

CALIFORNIA INSTITUTE OF TECHNOLOGY

PASADENA, CALIFORNIA

December 15, 1966

NATIONAL AERONAUTICS AND SPACE ADMINISTRATION

Technical Report No. 32-1037

The Design and Testing of an Inflated Sphere Impact Limiter

R. G. Ross, Jr.
W. E. Layman

Approved by:

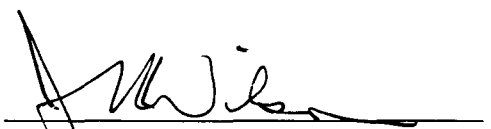

J. N. Wilson, *Manager*
Voyager Development

JET PROPULSION LABORATORY
CALIFORNIA INSTITUTE OF TECHNOLOGY
PASADENA, CALIFORNIA

December 15, 1966

Copyright © 1966
Jet Propulsion Laboratory
California Institute of Technology

Prepared Under Contract No. NAS 7-100
National Aeronautics & Space Administration

CONTENTS

I. Introduction 1

II. Structural and Geometric Requirements 2

III. Specific Design Problems 6
A. Overall Configuration 6
B. Convexities 8
C. Loading Webs 9
D. Cords 9

IV. Testing 12
A. Static Testing 12
B. Impact Test Facility 13
C. Prototype Test Results 13

V. Summary 19

Appendix: Derivations 19

Nomenclature 29

FIGURES

1. Effect of payload constraint on energy absorption 3
2. Effect of skin and cord inertia on cord tension 4
3. Convexity geometry for optimum cord loading 4
4. Limiting stable convexity shape 5
5. Limiter volume and weight vs number of convexities 5
6. Fabrication of test limiter 7
7. Completed limiter 8
8. Convexity shape and construction detail 10
9. Loading web and cord detail 11
10. Convexity ultimate pressure load test 12
11. Impact test facility 13
12. Pneumatic cannon and launcher basket 14
13. Test tank interior with limiter in launcher 15
14. Launcher extended and catch screen down 16

FIGURES (Cont'd)

15. Impact limiter during 100-ft/sec launch 16
16. Impact limiter contacting target, 100-ft/sec 17
17. Impact limiter fully deflected, 100-ft/sec 18
A-1. Convexity intersection angle vs α 21
A-2. Convexity intersection angle vs number of convexities 22
A-3. Convexity area vs α 25
A-4. Length of loading webs vs α 27

ABSTRACT

Section II of this Report analyzes an inflated-sphere landing vehicle in terms of structural requirements and geometric configurations necessary to effect maximum utilization of the vehicle's energy-absorbing properties. The requirements for an optimum limiter are set forth in the concluding remarks and all important derivations are included in the Appendix. Section III discusses fabrication techniques developed during the construction of a prototype vehicle and specific recommendations are made for future fabrication. Section IV presents preliminary test results obtained by shooting a 5-ft diameter prototype impact limiter against a flat surface at velocities of 100 and 165 ft/sec. Impact testing was conducted in a large vacuum chamber fitted with a launching mechanism designed for the prototype impact limiter.

I. INTRODUCTION

Increasing interest in planetary exploration has placed more and more emphasis on the problem of landing an instrumented payload on the surface of a planet with very little atmosphere. In general there are two approaches to such a landing: a soft landing using vernier retrorockets or, alternatively, an impact limiter controlled hard landing, preceded by the use of a parachute or other terminal velocity limiter. For *first-look* landings where instrumentation can be designed for high impact decelerations, impact limiters offer considerable advantage over vernier retrorockets because of their greater simplicity and subsequent reliability. Early investigations have shown crushable balsa wood limiters to be remarkably reliable and considerably more efficient than other materials because of the low weight and high energy absorption properties of the wood. Recent studies, however, have shown spherical gas bag impact limiters to be considerably lighter than equivalent balsa limiters and thus, theoretically, to offer an advantage if they can be brought to an operational level.

In operation a payload is centrally suspended within a large, gas filled balloon by numerous radial cords. The balloon, which is shipped deflated to the immediate vicinity of a planet, is inflated after preliminary deceleration to subsonic velocity and falls toward the planet. Because of its large size it acts as a terminal decelerator, reducing the payload velocity to the terminal velocity of the balloon. Upon impact the energy is absorbed by compressing the gas within the balloon which is in turn

ruptured just as the payload comes to rest, thereby freeing the payload and preventing rebound.

Many problems must be worked out before a spherical gas bag limiter can be made operational. Of primary importance among these is the verification of the theoretical predictions concerning the weight and energy-absorbing properties of the limiter. For this to be accomplished a working limiter must be designed and constructed. The following Sections deal with the overall structural and geometric requirements of the pneumatic limiter, the detailed fabrication techniques used to construct a working limiter, and the preliminary test results obtained by shooting the limiter against a flat surface at 100 and 165 ft/sec.

II. STRUCTURAL AND GEOMETRIC REQUIREMENTS

Consider an omni-directional impact limiter consisting of a large, gas filled, inelastic sphere within which the payload is centrally suspended by numerous radial cords. As the limiter impacts a hard flat surface, the kinetic energy of the payload and skin is transferred to the gas by compressing the gas between the impacted surface and the restrained skin. Since the contained gas is weightwise a far more efficient absorber of energy than the limiter's structural materials, the structure is made of materials with as high an elastic modulus as possible so that the majority of the energy is transferred to the gas. In order to examine the efficiency of a limiter of a given physical size, made of inelastic materials, let us define the most efficient limiter as the limiter which will absorb the most kinetic energy without exceeding some maximum deceleration level. It can thus be noted, Fig. 1, that since the magnitude of the kinetic energy absorbed is equal to the integral of the contact force through the decelerating distance of the center of gravity (cg), the most efficient limiter construction will be that which results in the largest average contact force during the maximum allowable cg movement, Derivation No. 1.[1] Since the mass of the limiter is small relative to that of the payload, the center of gravity is approximately coincident with that of the payload. Thus the cg movement can be broken into two components: the motion of the payload relative to the limiter, and the motion of the limiter relative to the impacted surface. Because the contact force is predominantly controlled by the latter, however, any motion of the payload relative to the limiter absorbs considerably less energy than an equivalent motion of the limiter as a whole. This implies that an efficient limiter must be able to transfer the decelerating load to the payload from the skin with a minimum of relative movement between the two. This relative movement arises if the initial configuration of the skin is not the same as that required to support the maximum cord loads during impact.

It is thus reasonable to say, after considering the above, that the most efficient limiter will be made of inextensible materials and will have a skin configuration prior to impact which is the same all over as that required to support the maximum cord loads during impact. With such a configuration and with inextensible cords and skin, it is reasonable to assume also that the tension in all cords except those within the contact area will have approximately equal tensions. This is because a given skin configuration automatically applies a fixed proportion of the pressure load to the cords; and, with inextensible cords and skin, it seems logical that the skin configuration would be resistant to change. In order to get an idea of the required skin configuration for minimum payload relative motion, consider a spherical limiter of radius R whose skin and cord weight is negligible with respect to that of the payload. Also assume that the skin configuration is such that the payload stays coincident with the center of the limiter during impact, and that internal pressure P stresses each cord equally. In this limiting case, it can be shown that the instantaneous tension f in each of the N equally-spaced cords is $f = 4\pi R^2 P/N$, Derivation No. 2. Thus a total evenly-distributed force of $4\pi R^2 P$ must be applied to the payload during the act of impact. This is seen to be the pressure multiplied by the total surface area of the limiter and thus, with closely

[1] Derivations Nos. 1-10 refer to Derivation Numbers in the Appendix.

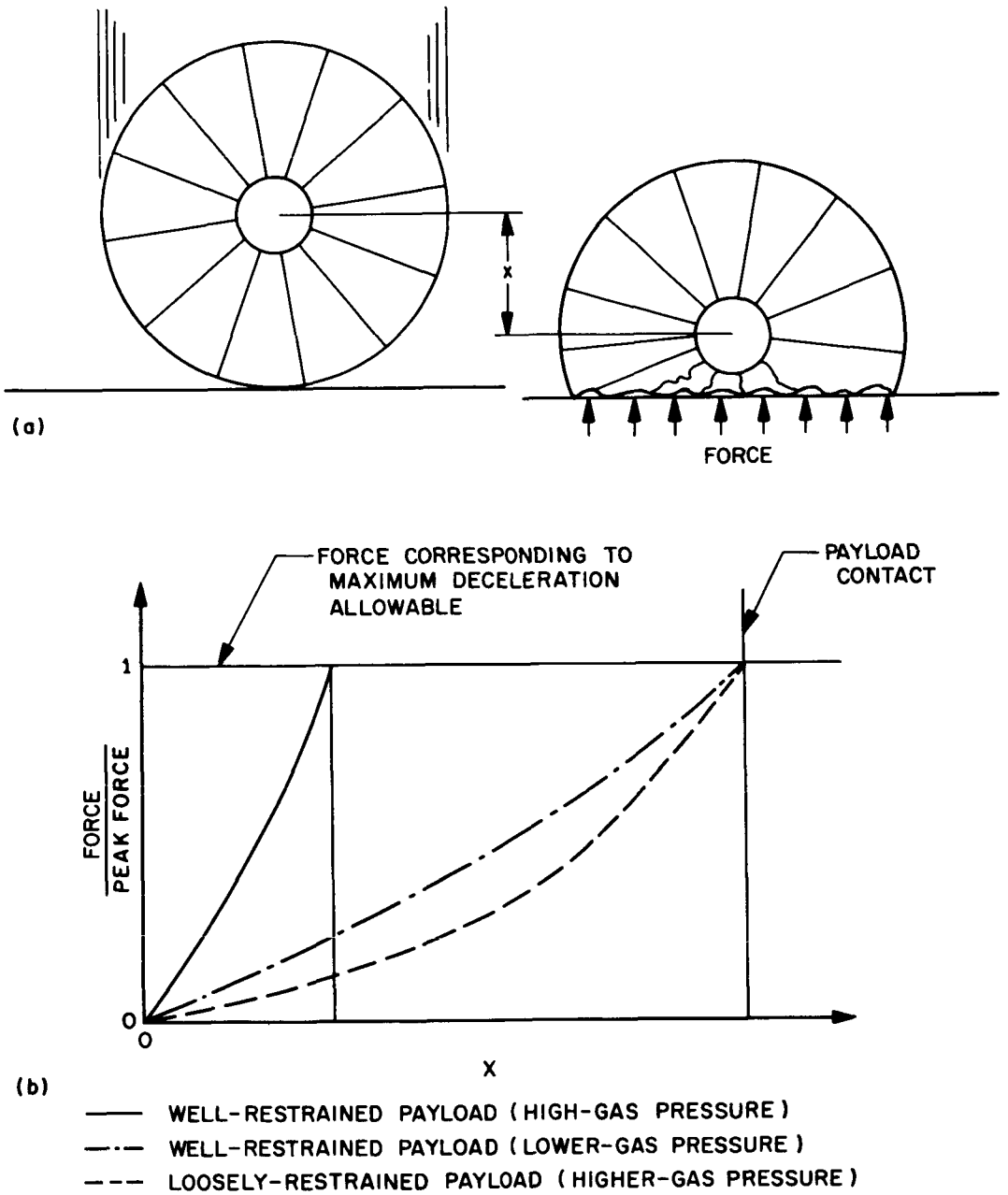

Fig. 1. Effect of payload constraint on energy absorption

spaced cords, is the maximum force the gas pressure will support. This implies that in the limit, for no relative motion between the payload and skin, the cords must fully support the internal pressure, with none being supported by circumferential hoop stresses in the skin. If the cords are fully supporting the gas pressure, then each cord will by necessity be equally stressed both before and during impact except of course those in the contact area. Thus with a skin designed to load the cords completely, the impact load is transferred to the payload by the releasing of tension in the cords of the contact area together with the increasing tension in the remaining cords due to increasing gas pressure.

If the skin is not designed to fully load the cords, then the required deceleration load will be transferred to the payload only after the skin has been pulled into a configuration which will support the load. Such distortion implies that the payload will move off center while loading the skin, thereby inefficiently using the allowable

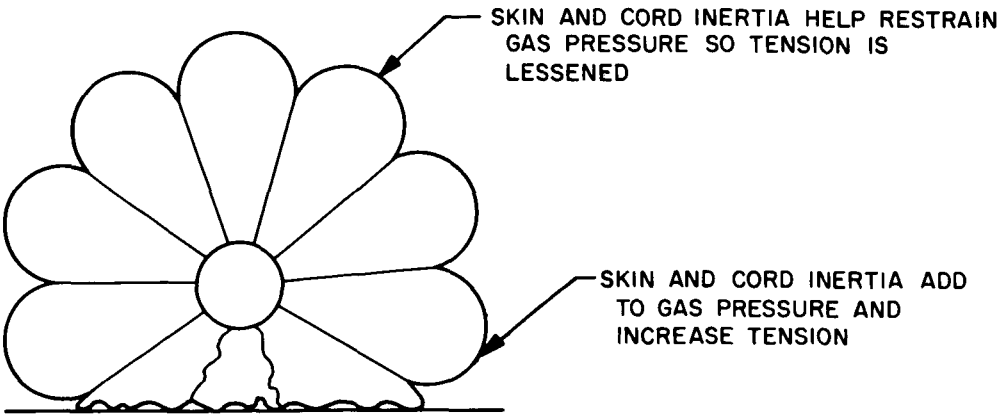

Fig. 2. Effect of skin and cord inertia on cord tension

decelerating distance before payload impact, and thus decreasing the energy absorption of the limiter. The same is true if the supporting cords have an appreciable elongation during impact.

In the realistic case, the skin and cord weight will not be negligible as assumed above but will amount to about 20% of the total weight. This probably will not change the required configuration because, as shown in Fig. 2, the inertia of the skin will automatically tend to lessen the force applied to the payload in proportion to the loss in payload weight. Thus, to a first approximation, it appears that the optimum skin configuration will apply a total evenly-distributed force equal to $4\pi R^2 P$ to the payload. For closely-spaced cords, this implies that all circumferential hoop stresses which provide overall skin restraint must be eliminated so that the cords can absorb the total pressure load.

In the light of this fact, it is assumed that the cords cannot be fastened individually as point loads directly to the skin because this would allow a network of hoop stresses to weave between the cord attach points. The cords must then be fastened in groups along webs so that line loads are applied in a way that will divide the skin surface into a large number of convex areas (convexities), each of which must be completely restrained by the cords fastened to its perimeter. In order for these convexities to transfer a total evenly-distributed force of $4\pi R^2 P$ to the cords, Derivation No. 3 shows that the surfaces of adjacent convexities must intersect with an angle θ approximately equal to ¼ of the angle subtended by a single convexity, Fig. 3. For more than 30 convexities, the required intersection angle is less than 10 deg and thus implies that the convexities of an optimum limiter are approximately tangent to one another.

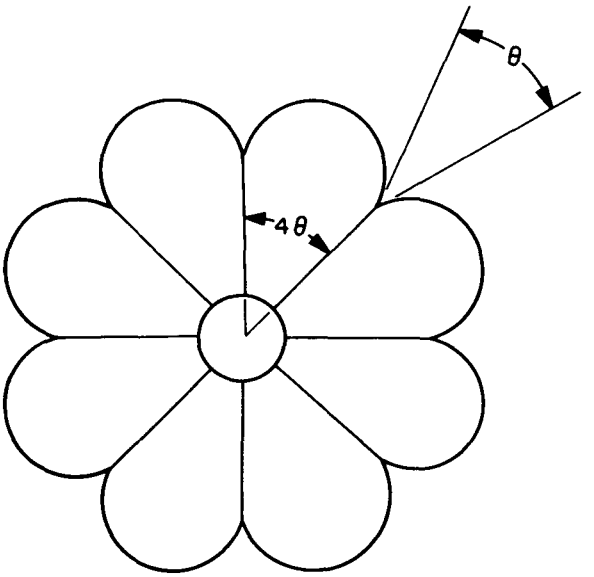

Fig. 3. Convexity geometry for optimum cord loading

In order for this angular requirement to be successfully realized, however, each convexity in itself must be a surface whose equilibrium configuration while inflated meets the angular requirements. An optimum limiter must also minimize surface area, because minimum weight is of utmost importance in the limiter design. Thus each convexity should be constructed with a configuration which minimizes surface area while continuing to meet angular stability and strength requirements. If we assume that each of the convexities is approximately the same size and has an approximately circular perimeter, Derivation No. 4 shows that the limiting stable shape will be a section of the flattened sphere shown in Fig. 4. This shape has the minimum surface area for a given diameter but has the disadvantage of having infinitely increasing stresses at its dome. These high

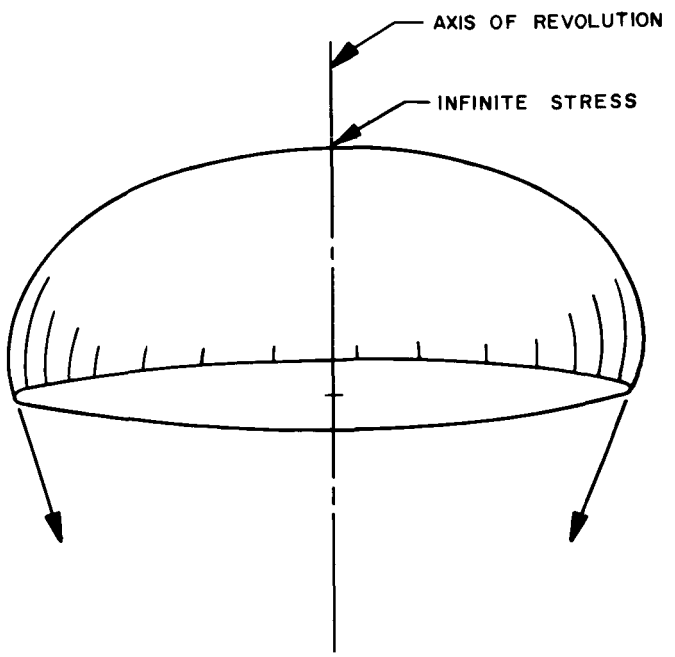

Fig. 4. Limiting stable convexity shape

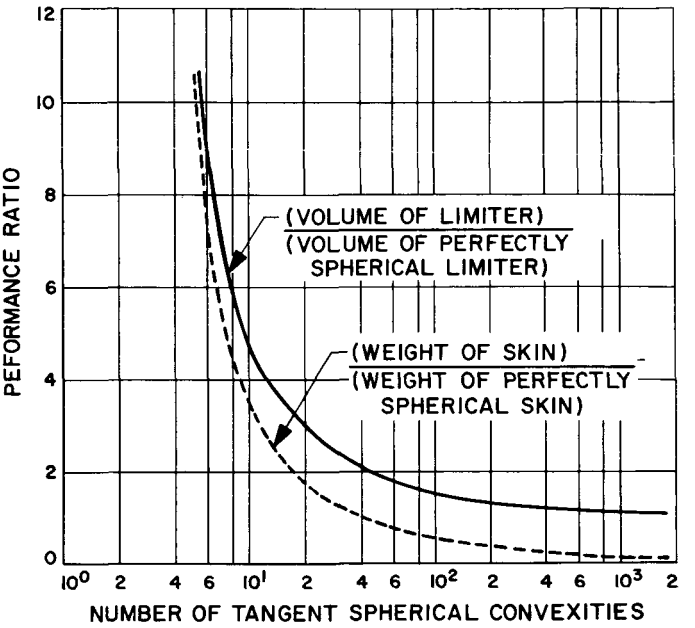

Fig. 5. Limiter volume and weight vs number of convexities

stresses, due to the absence of hoop stresses parallel to the equatorial plane, make the shape unusable from a strength standpoint, and thus the optimum shape for the convexities of the limiter will lie somewhere beween this shape and a true sphere.[2] Thus, on the basis of the above argument, the limiter should be made up of a number of approximatcly spherical convexities, each approximately tangent to one another.

The bulbous convexity creates two departures from the spherical model. First, it radically alters the strength and surface area of the limiter, Derivation No. 5, and thus the weight, Derivation No. 6; and second, it adds considerable volume without increasing the maximum cord load, which increases the energy storage capacity of the limiter without increasing its payload support ability. As shown in Fig. 5, the skin weight of the limiter decreases quite rapidly with increasing numbers of convexities and is actually less than that for a perfectly spherical skin when the surface is divided into more than 40 spherical convexities. Of course, the total limiter weight will also include that of the cords and loading webs; unlike the skin weight, however, these are almost independent of geometry. This is because the total pressure load is only a function of the ID of the limiter and is not a function of surface area. Since both the strength and weight of a given-length tension member are proportional to its area, the weight of cords is thus a constant. A similar argument holds for the weight of the loading web since its required weight per unit length decreases at the same rate the total required length increases with increasing numbers of convexities.

From this discussion it can be seen that the variation in skin weight due to using the convexities offers a weight *advantage* provided that the skin is divided into more than about 40 convexities.

The effect of the increased limiter volume also shows advantages. Since the OD of the limiter is greater than that of a perfectly spherical limiter, the allowable compression stroke before payload impact is obviously increased. This increase in stroke combined with approximately the same cord loads thus implies an increase in energy absorbing ability for the same or less structural weight, i.e., a higher efficiency. The variation of efficiency with number of convexities is not well understood but, if the energy storage ability is proportional to the limiter's total volume as for a pure sphere, it appears from the graph that the efficiency increases as the number of convexities increases, i.e., the ratio of energy storage volume-to-skin weight appears to maximize with increasing convexities.

[2] A true sphere is the optimum shape, from a strength standpoint.

The optimum impact limiter thus appears to be made up of at least 40 quasispherical convexities, all approximately tangent to one another and forming a large spherical skin. The payload is fastened to the skin by a large number of inextensible cords fastened via loading webs to the lines of intersection of the convexities. The number of cords used is based primarily on reducing the local skin load at the point of cord connection to within acceptable levels and on evenly supporting each convexity. Both the skin and the cords should be made of materials with high strength, low weight, and high resistance to elongation.

For limiters with less than 40 convexities, it may be advantageous to enlarge the intersection angle between convexities in order to decrease the excessive surface area and unsupported volume. However, the effect of this on the limiter efficiency is not yet well understood.

III. SPECIFIC DESIGN PROBLEMS

In Section II, an inflated impact limiter was analyzed in terms of structural requirements and geometric configurations necessary to effect maximum utilization of the vehicle's energy absorbing properties. In this Section III, fabrication techniques developed during the construction of a prototype vehicle are discussed and specific recommendations are made for future fabrication. In order to clarify the presentation, the fabrication problems have been grouped into four sub-sections: 1) those dealing with the overall configuration, 2) those dealing with the convexities, 3) those dealing with the loading webs, and 4) those dealing with the cords.

A. Overall Configuration

The optimum configuration for a gas-filled sphere impact limiter as described in Section II is a large skin made up of at least 40 quasi-spherical convexities all approximately tangent to one another. The skin is fastened to the payload by a large number of inextensible cords via loading webs bonded to the intersection lines of the convexities. Of course, the surface of an actual sphere cannot be divided into a number of spherical convexities, each tangent to those adjacent to it, for geometric reasons. The sphere can however be approximated by any one of an infinite number of polyhedra. For simplicity, a regular polyhedron with all sides symmetrical would be best, but the maximum number of sides available on a regular polyhedron is 20 (icosahedron), and the next best is 12 (dodecahedron).

The triangular sides of the icosahedron complicate the construction of convexities and make this shape undesirable. The pentagonal sides of the dodecahedron simplify the construction of convexities, but the low number of faces results in a severe weight penalty. A configuration which shows great promise is the polyhedron obtained by cutting off each of the 12 vertices of an icosahedron. This results in a polyhedron with 12 symetrically-spaced pentagonal sides between 20 hexagonal sides. By varying the amount of the vertex that is truncated, the pentagonal side can be varied in size so that its load per unit length of perimeter is the same as that of the adjacent hexagonal sides.

Another similar polyhedron can be obtained by making 30 hexagonal sides on the edges of a dodecahedron connected with 12 small pentagonal sides parallel to and symmetrical with the original large pentagonal sides of the dodecahedron; the hexagons are placed such that two opposing vertices of each hexagon are coincident with two adjacent vertices of the dodecahedron. For a first model, however, it was felt that the geometry should be kept as simple as possible since verification of construction techniques and the theory in Section II were the primary objectives. For this reason, it was decided to base the first model on the dodecahedron shape. This gave a limiter with 12 equal convexities, each with a pentagonal perimeter and thus gave 30 intersection lines to which the loading webs could be bonded, Fig. 6 and 7. The model payload was made by simply threading 30 eyes into a solid aluminum sphere such that each eye was directly under one of the 30 loading webs.

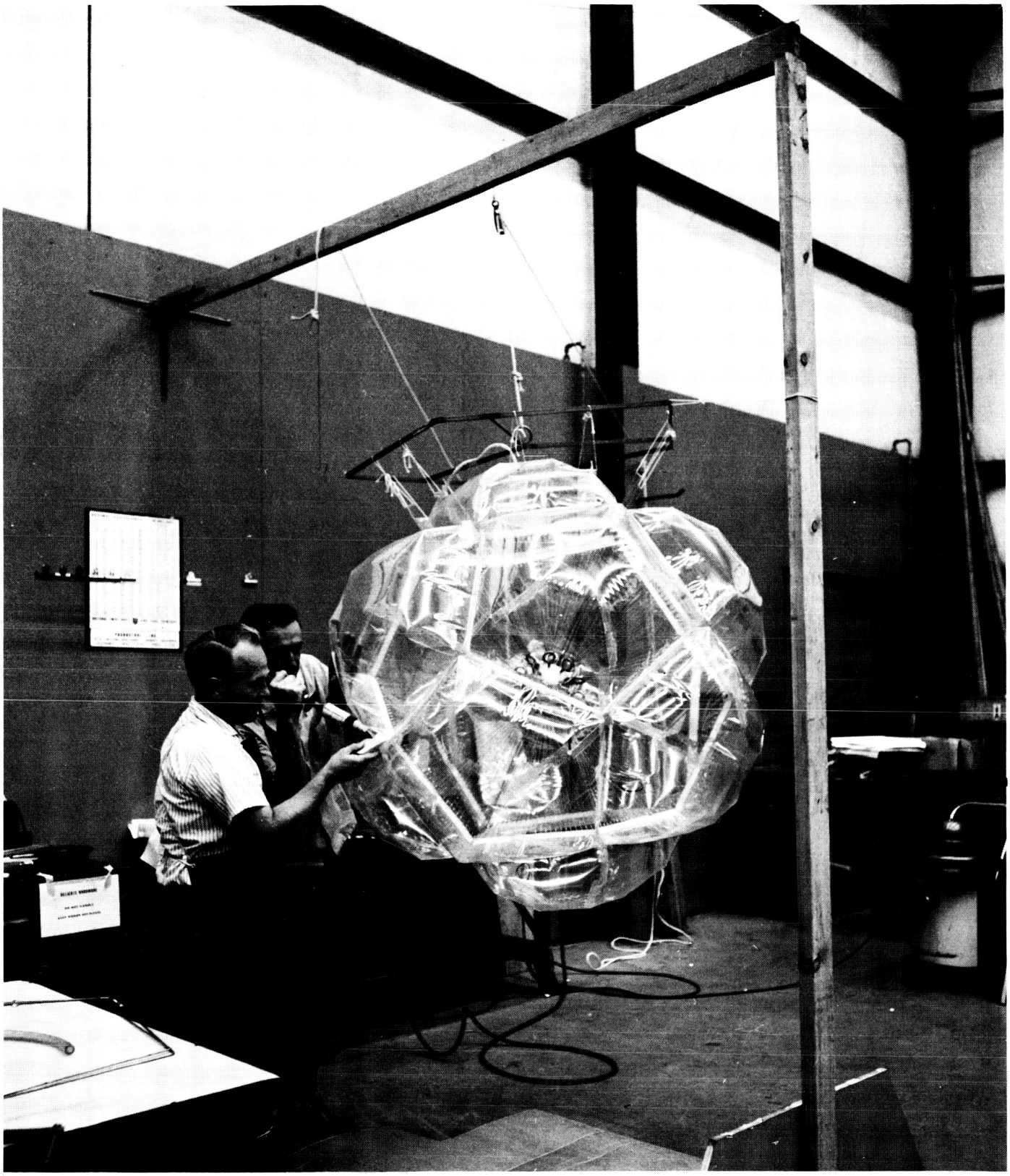

Fig. 6. Fabrication of test limiter

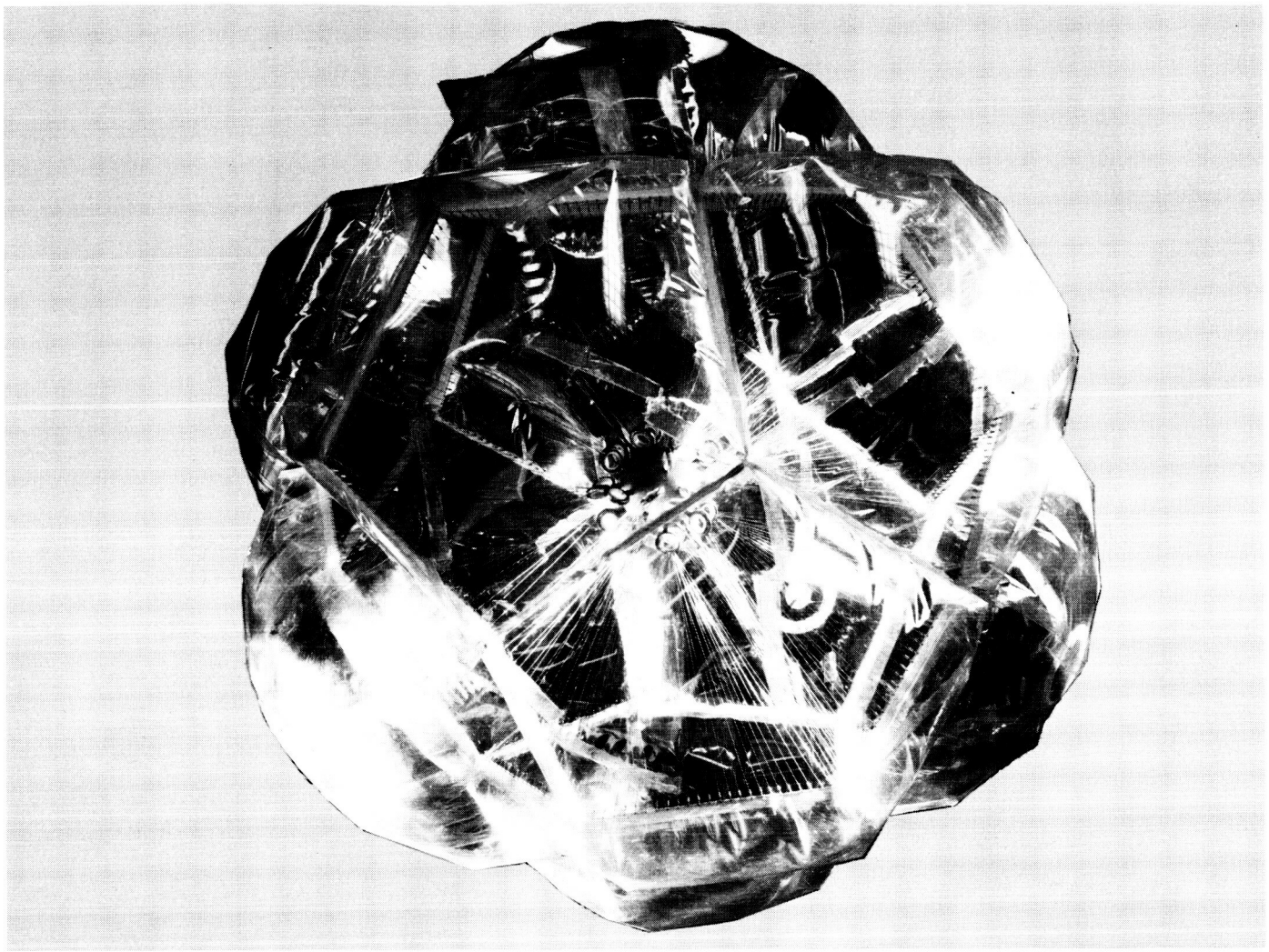

Fig. 7. Completed limiter

For future limiters, however, it is felt that a larger number of convexities would be desirable in order to more closely approximate the ideal limiter as described in Section II. Either of the two previously mentioned pentagon-hexagon combination polyhedrons is a possible configuration.

The overall size of the limiter can be chosen by either of two ways or both. First, the volume and weight of the skin can be approximated by an equivalent sphere and the size relationships determined from information in NASA Technical Note D-692, compiled by E. Dale Martin of Ames Research Center. Or second, the size, weight, and volume can be calculated with the help of Derivations No. 6 and 7 and Fig. 5 in Section II, and then the kinetic energy of the resulting limiter can be compared with its allowable energy absorption as calculated from an isentropic volume change.[3] The latter of the two will obviously require several iterations but is considerably more accurate. The optimum method is probably to get a first guess from the NASA Technical Note, and then to converge to a more accurate estimate using the second method.

B. Convexities

In the design of the convexities, four problems were considered: 1) what type of material to be used, 2) how

[3] The expression for the allowable energy absorption from an isentropic volume change is included as Derivation No. 10 in the Appendix.

strong the convexities must be, 3) what shape the convexities should have, and 4) the optimum fabrication method.

The material for the convexities first of all had to have as high a strength-to-weight ratio as possible and second, it had to be inelastic enough not to grossly deform when pressurized. A moderate degree of elasticity or plasticity was felt to be necessary in order to ensure the relief of stress concentrations. Mylar was chosen as the test material largely because of its superior strength and clarity properties; these permitted photographic studies of payload motion inside the limiter. For skins where visual clarity is not required, it was felt that one of the many mylar-backed nylon cloths would be best because of their superior rip resistance, and strength properties.

The strength requirements of the mylar were calculated by approximating the convexity as the section of a sphere and using the standard expression for the biaxial stress in a pressurized sphere. Since the convexities were actually sections of a polyhedron, this technique had obvious inherent inaccuracies. It was felt, however, that this technique would yield approximate figures that could be refined by actual testing and that the unpredictability of the shape of the pressurized convexities did not warrant more exacting analysis.

The actual shape of the convexities was primarily determined by fabrication limitations. The general shape, though, was more or less an intuitive guess. As explained in Section II, the optimum shape for convexities is the section of a sphere, the sphere being sized so that neighboring convexities are approximately tangent. With only 12 convexities, however, tangent spherical convexities would nearly quadruple the limiter volume and nearly triple the weight of the skin. This increase in volume would, in turn, radically change the limiter's energy absorbing ability and would result in an obviously unrealistic structure. It was thus decided to make the unpressurized shape of the convexities half way between what was guessed to be the pressurized shape and the expected shape during impact. The shape is shown in Fig. 8.

Due to limited fabrication facilities at hand, it was decided that the convexities would have to be manufactured from flat patterns. The resistance to yielding of the mylar during fabrication also added the restriction that all seams be straight lines and thus that a convexity actually be the section of a polyhedron. The general convexity shape decided upon was thus approximated by a polyhedron which was in turn reduced to a flat pattern. After some experimenting with adhesives, it was decided that "iron-on" thermo plastic tape adhesive GT-100, manufactured by the Schjeldahl Co., gave consistent and strong seams while also simplifying manufacturing problems considerably, due to its instant curing properties.

On future limiters, it is felt that the number of convexities should be increased to 40 or 50 so that the convexities can be made approximately spherical in shape without adversely affecting the overall energy-absorbing ability of the limiter.

C. Loading Webs

The primary purpose of the loading webs is to transfer the point loads of the cords into line loads on the skin. Thus besides having a high strength-to-weight ratio, they must be extremely resistant to tearing and must be tough enough to dissipate the point loads without local failure. Because all adhesives tried had very low peel strength, the webs had to be constructed so that all joints were loaded in shear. Since the limiter skin is badly deformed during impact, it was also felt that the webs should be made as shallow as possible so that bending stiffness of the seams could be kept to a minimum. After considerable testing, it was found that a nylon line bonded into a mylar-backed nylon fabric web had superior strength and flexibility properties, Fig. 9. To obtain a strong bond between the nylon mono-filament and the fabric, a special heat-sealing fixture had to be designed. This heating fixture clamped the fabric about the nylon line and heated the web to the curing temperature of the thermoplastic adhesive. The resulting web was trimmed to size and holes were melted at equal intervals along the web for connecting the radial cords. The webs were then bonded to the finished seams between convexities using the same thermoplastic adhesive.

D. Cords

As explained in Section II, the two primary properties of the cords are: 1) high strength-to-weight ratio, and 2) high resistance to elongation. The high strength-to-weight ratio, together with the obvious requirement that the cords not be brittle, limited the material choice to either nylon mono-filament or music wire. Although the nylon has a 50% better strength-to-weight ratio than the wire, its elastic modulus is magnitudes lower than that of steel and thus even with a considerably larger cross-

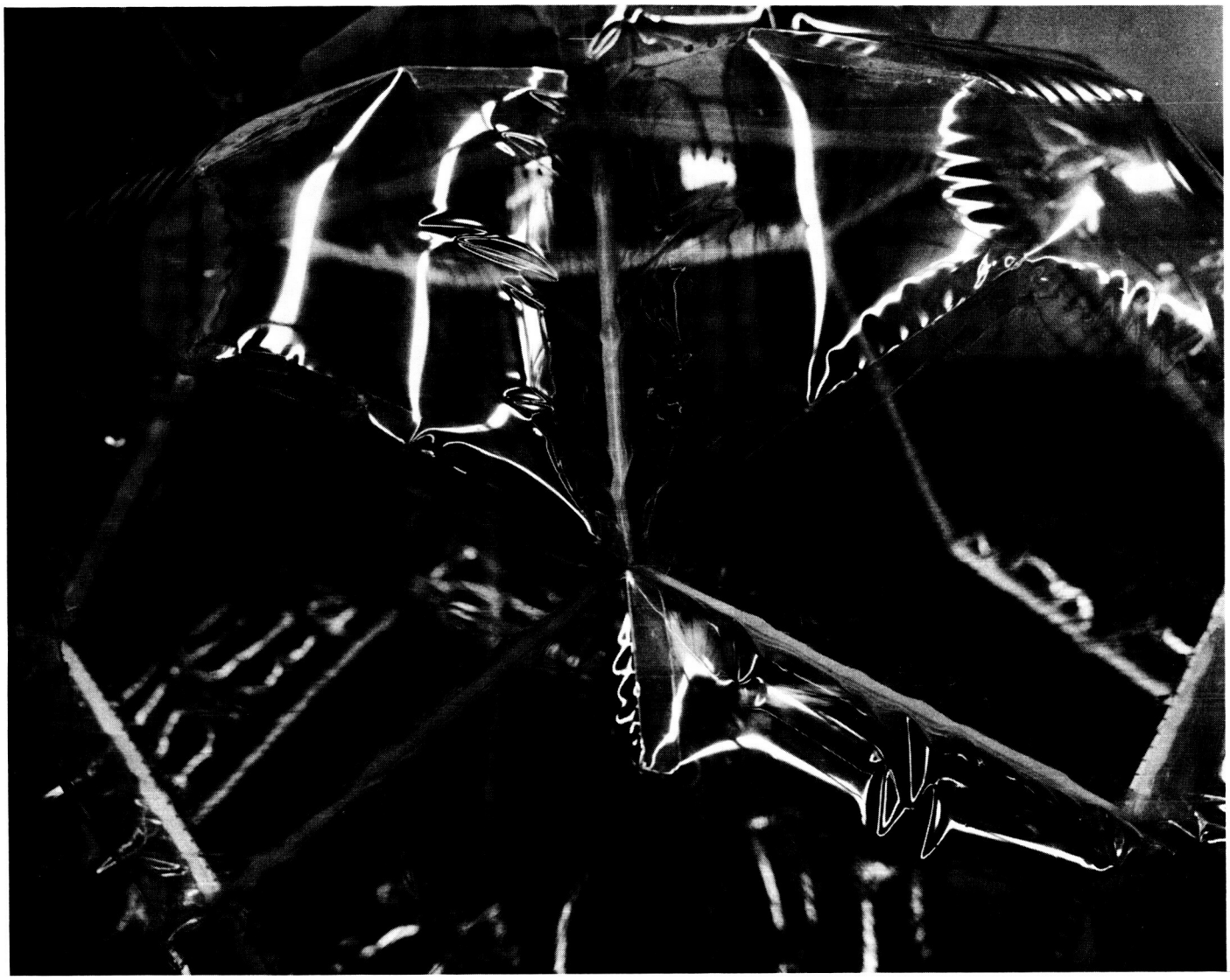

Fig. 8. Convexity shape and construction detail

sectional area has very inferior stiffness properties. Music wire was thus chosen as the cord material. A glass filament reinforced cord could be manufactured to provide a nonmetallic high stiffness cord if this were desirable.

Because of the manufacturing problems connected with tying large numbers of cords, it was decided that the fastening method should be as simple as possible consistent with weight and strength. A crimp sleeve fastener was thus almost immediately chosen as the fastening technique. After some experimenting, it was found that the crimp sleeve had to have a very heavy wall in order to retain enough preload to keep the music wire from slipping under load. Even then it was found that the loose wire end needed to be bent back over the sleeve to prevent the wire from slipping, Fig. 9.

Because of the small diameter of the wire, it was also found necessary to pass the wire through stainless steel tubing at the web attach point in order to distribute the tension load more evenly onto the loading webs.

The number of wires used was primarily decided by the strength of the loading webs combined with making sure that the convexities were more or less evenly loaded. It was decided that one wire about each ⅝ in. would be adequate and thus it was decided to place 24 wires along each of the 30 loading webs, making a total of 720 wires.

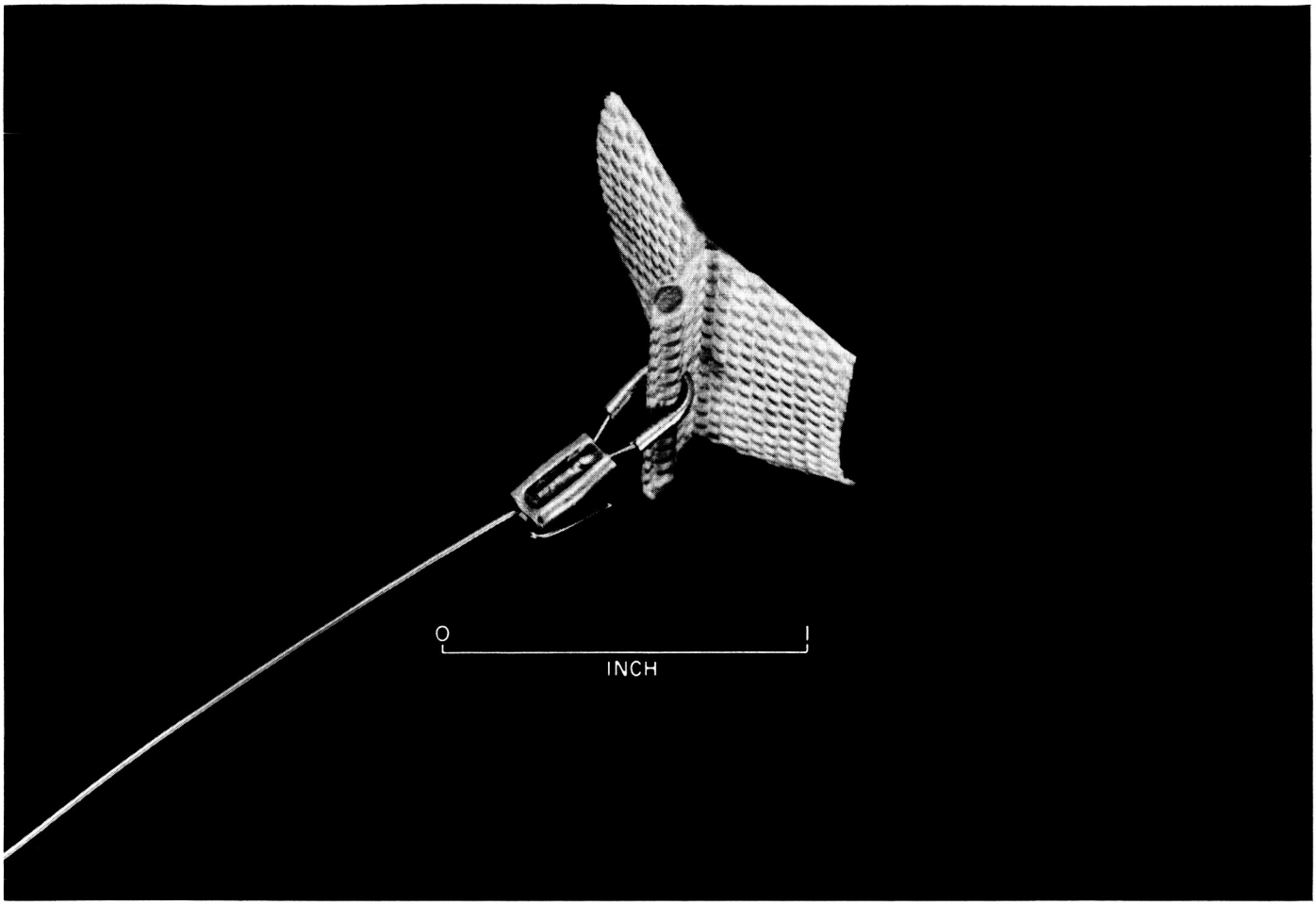

Fig. 9. Loading web and cord detail

It might be noted here that defining a given payload weight and a given impact velocity does not define a unique diameter for the pneumatic impact limiter sphere. The definition of payload weight and velocity does define a unique impact limiter weight, but this weight may be realized in a very large diameter sphere with thin skins and long light-gauge payload support wires, or in a small diameter sphere with thick skins and short heavy-gauge payload support wires. The 5-ft diameter of the prototype limiter described above was chosen as a maximum reasonable size capable of being tested in a vacuum chamber. The 200-ft/sec design impact velocity was chosen as representative of the velocities encountered in typical planetary landing systems, and the 12.2-lb payload was chosen to make the impact limiter skin thickness (5 mils) fall into a workable range for fabrication without developing special techniques.[4]

[4] As a point of reference a 250-lb payload could be protected from a 150-ft/sec impact by a 25-ft diameter impact limiter having a skin thickness of approximately 1 mil.

IV. TESTING

The prototype impact limiter described in Section III was tested at the component level with static loads and was then tested in vacuum as a completed assembly with actual impact tests at a velocity of 100 ft/sec, then at 165 ft/sec.

A. Static Testing

Two preliminary static tests were conducted, one to validate the payload support cord and web design, and a second to validate the convex dome (convexity) design. The static testing of the web and payload support cord assembly was accomplished by bonding a 24-cord web assembly to a sheet of 5-mil mylar, and then attaching the mylar to one platen of a tensile testing machine; Fig. 9 shows a short section of web. Payload support cords attached the web to an eyebolt which was secured to the opposite platen of the tensile testing machine. Early tests produced web failures at total loads of 1,250 lb or an equivalent impact limiter gas pressure of 7.8 psi. The web failures in these tests were due to slippage of the payload support cords through their crimp collar attachments. An improved crimp collar technique was then developed which increased the web failure load equivalent pressure to 11.2 psi. This improved design was used in the fabrication of the prototype impact limiter. As a point of reference the prototype impact limiter internal gas pressure would reach 10.6 psi during a 200-ft/sec impact.

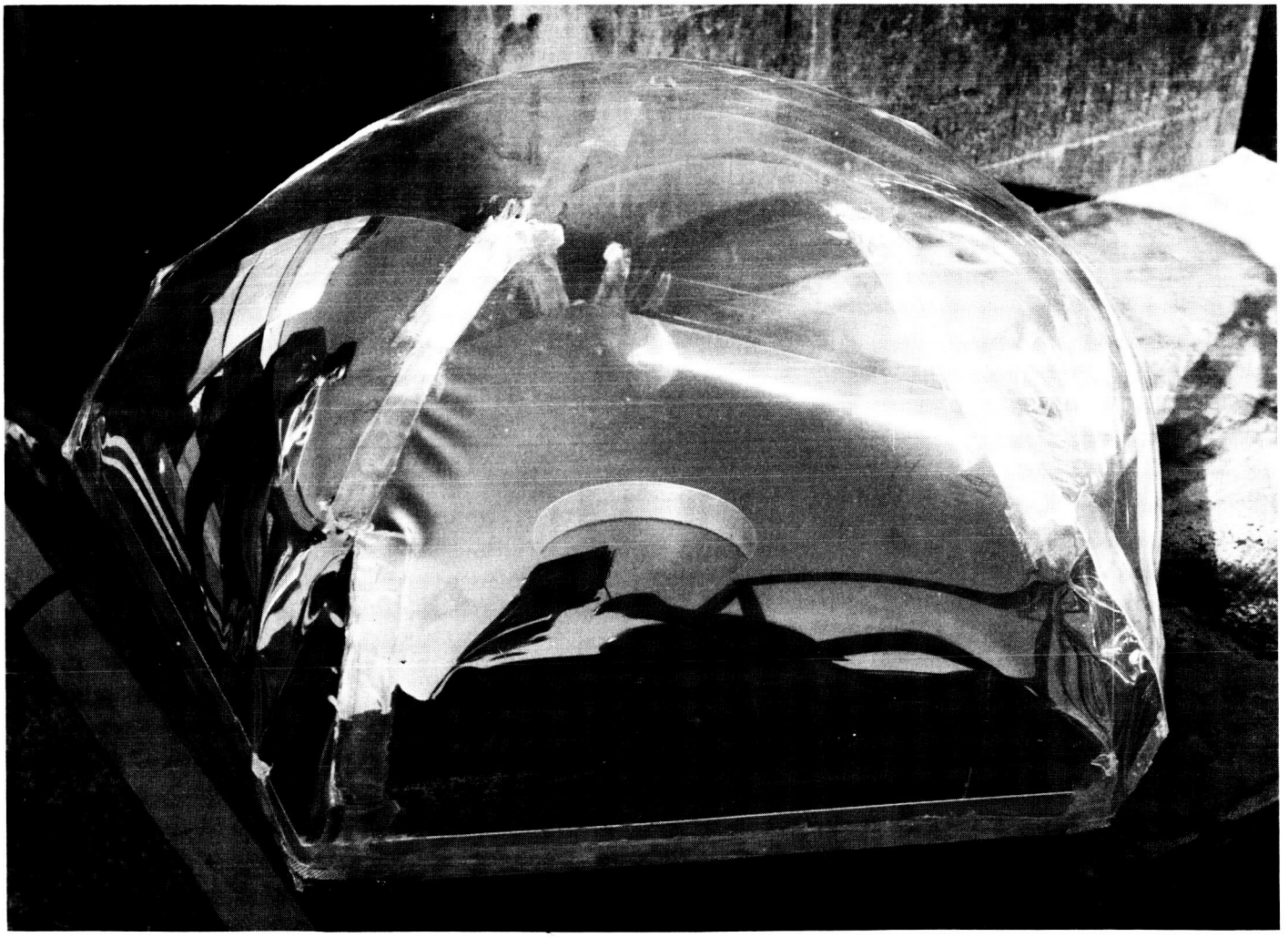

Fig. 10. Convexity ultimate pressure load test

The static testing of the convex dome design was accomplished by attaching one of the mylar domes to a flat plate, Fig. 10, and pressurizing it to failure. The dome failed at approximately 12.5 psi or a total force per dome of approximately 7,000 lb. This agreed very well with the analytic prediction of 12 psi, and the tested dome design was incorporated into the prototype impact limiter fabrication.

B. Impact Test Facility

The dynamic testing of the prototype pneumatic impact limiter was accomplished in a 10-ft diameter, 25-ft-long horizontal vacuum chamber. The launching of the limiter was done by a pneumatic *cannon* mounted outside the chamber and driving a launch basket via a ram running through a seal at the end of the chamber; see Fig. 11 (Test Facility), and Fig. 12 (Pneumatic Cannon). The test chamber floor was illuminated by 14 kw of quartz lamps and the impact area at the end of the tank by eight PH-31 flash bulbs which were timer-ignited 25 msec prior to impact and remained lighted for 50 msec. Motion picture camera coverage was provided by two very wide-angle, 500-frame/sec Milliken cameras which provided overlapping views of the launch and the trajectory to the target. Additional coverage was provided by a 7000-frame/sec, wide-angle Fastax camera which viewed the actual impact. All photography was silhouette photography in which the limiter was viewed against a bright background and very little light fell directly on the limiter. With a given amount of light, this technique allowed the cameras to be set for a great depth of field and also allowed high resolution *slow* film to be used in recording the action. The photographic advantages of this silhouette technique were due to the high contrast between subject and background inherent in a silhouette. The high contrast provided good subject definition even though the film was severely underexposed.

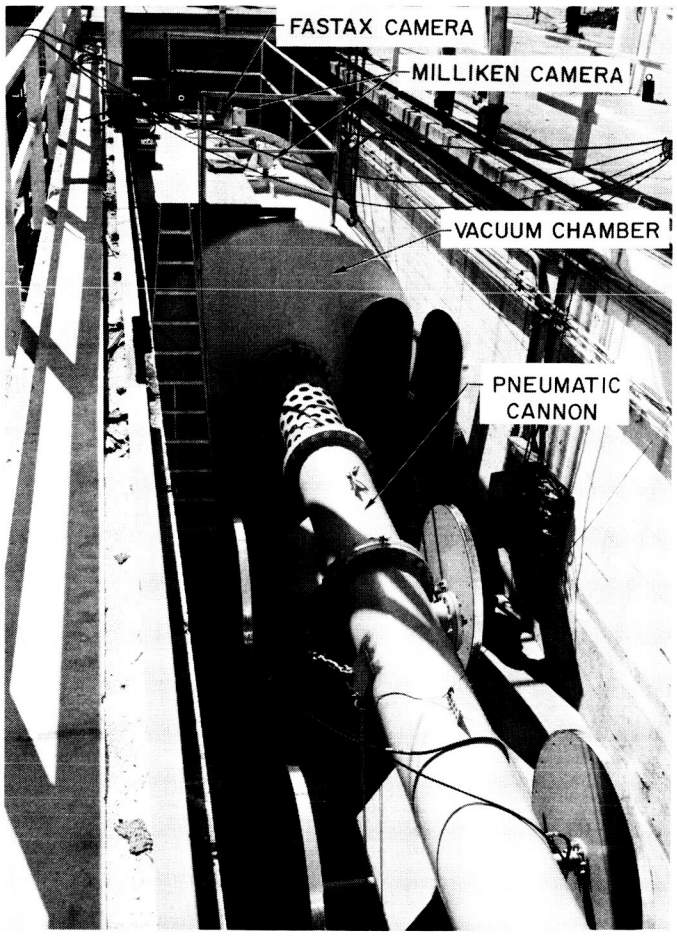

Fig. 11. Impact test facility

In addition to the cameras, lights, and launcher, the test chamber also contained a chain link fence catch screen, seen at the top of the tank in Fig. 13, which slammed down after the impact limiter passed the center of the tank and prevented the limiter from rebounding into the launcher basket. Figure 14 shows postlaunch configuration, launcher at full stroke, catch screen down.

C. Prototype Test Results

The prototype impact limiter described in Section III was installed in the vacuum test facility and launched in vacuum, Fig. 15, at 100 ft/sec while internally pressurized[5] at 2 psi. The limiter impacted on a vertex of its base dodecahedron, Fig. 16, worked properly and stopped the payload approximately 6 in. short of the target, Fig. 17. An accurate comparison of test limiter deflection with analytically predicted limiter deflection is not readily feasible because the analysis assumed a 48-in. mean spherical diameter rather than numerically integrating the stroke and volume effects caused by the domes of the limiter. The analysis allowed a stroke of 0.8 R and an effective limiter radius R of 24 in. to approximate the prototype limiter which had twelve domes, each of 10 in. effective radius, on the faces of a dodecahedron measuring 40 in. across the flats. The assumption of a 48-in. effective spherical diameter was slightly conservative, and although there was not time during the brief limiter development program for a

[5] Theoretical calculations indicated that a pressure of 1.83 psi would stop the internal payload just as the payload reached the target surface.

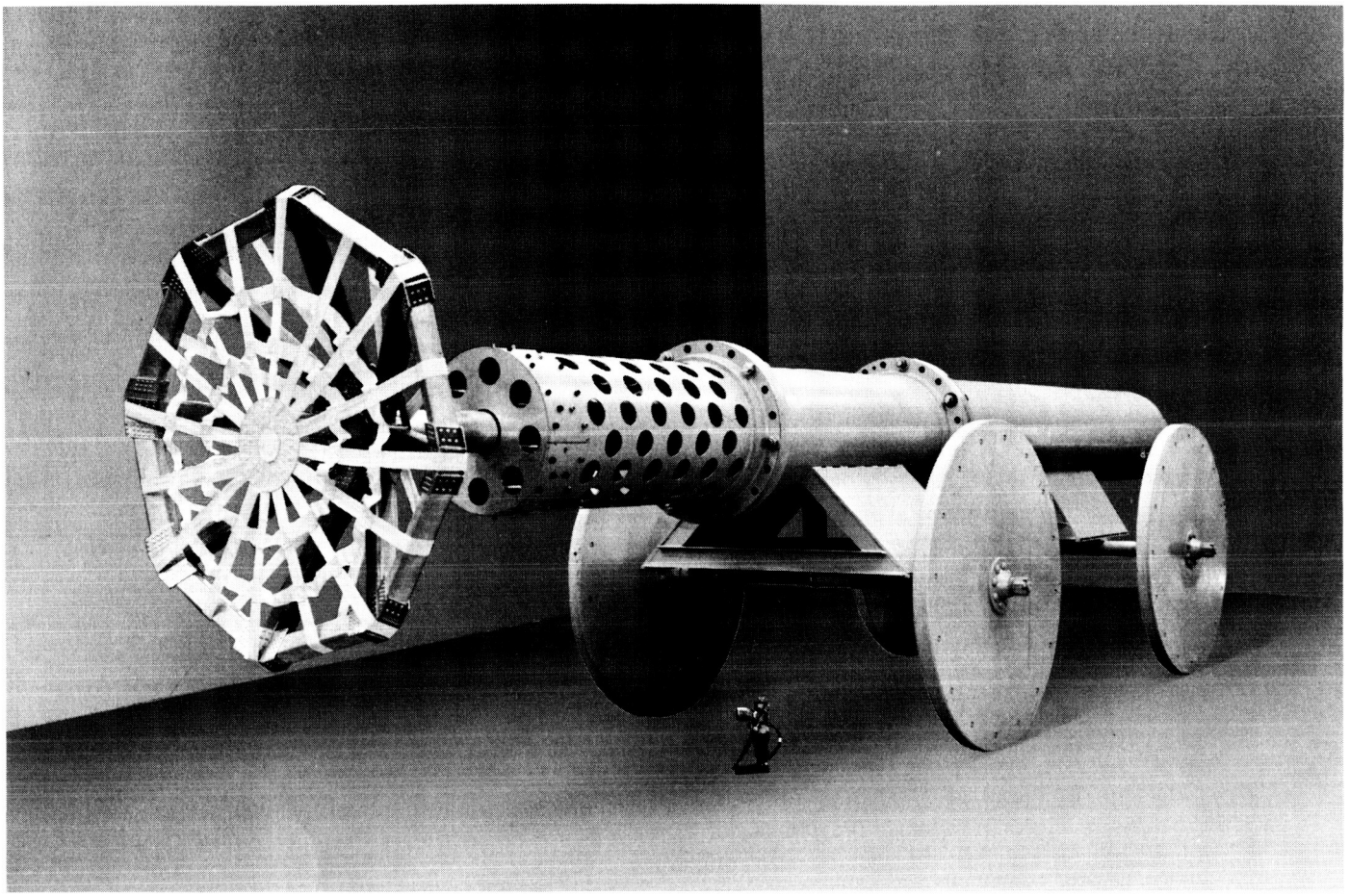

Fig. 12. Pneumatic cannon and launcher basket

detailed plot of impact limiter volume vs deflection, it is clear that a precision comparison of analysis with test data would require such a plot.

The developing and testing of prototype impact limiter was done primarily to unearth any unanticipated problems which might have remained hidden in a purely analytical study. Also, a secondary objective of the prototype program was to set a lower bound on pneumatic impact limiter efficiency, keeping in mind that design compromises would be made as necessary to simplify fabrication and testing.[6] Results of the fabrication and testing revealed no special problems other than the straightforward impact limiter design problems explained in Section III, and the limiter did function properly to establish an efficiency lower bound; this is described later in this Section.

After the prototype limiter had been tested at 100 ft/sec, it exhibited some fairly severe rips in the domes and also the dome-to-cord attachment webs showed signs of delamination. These damaged areas are thought to be the result of severe creasing during impact followed by the violent reexpansion accompanying rebound. Further damage was probably done as the impact limiter was trapped in the catch screen and hurled to the tank floor. Despite the damaged condition of the limiter, it was decided that a repair and retest at higher velocity should be attempted. The repair effort was limited to minor patching of the domes with no attempt being made to strengthen the overexercised webs.

After the repair, a second launching of the prototype limiter was conducted in the vacuum test facility at a velocity of 165 ft/sec with a limiter internal pressure[7] of 3.7 psi. Again the limiter worked properly, decelerating

[6] For instance, mylar film rather than nylon cloth skin was used; a factor-of-two skin weight penalty was taken to permit photography of the payload dynamics during impact.

[7] The analytically predicted minimum pressure for stopping the internal payload, just as it reached the impact surface, was 3.52 psi.

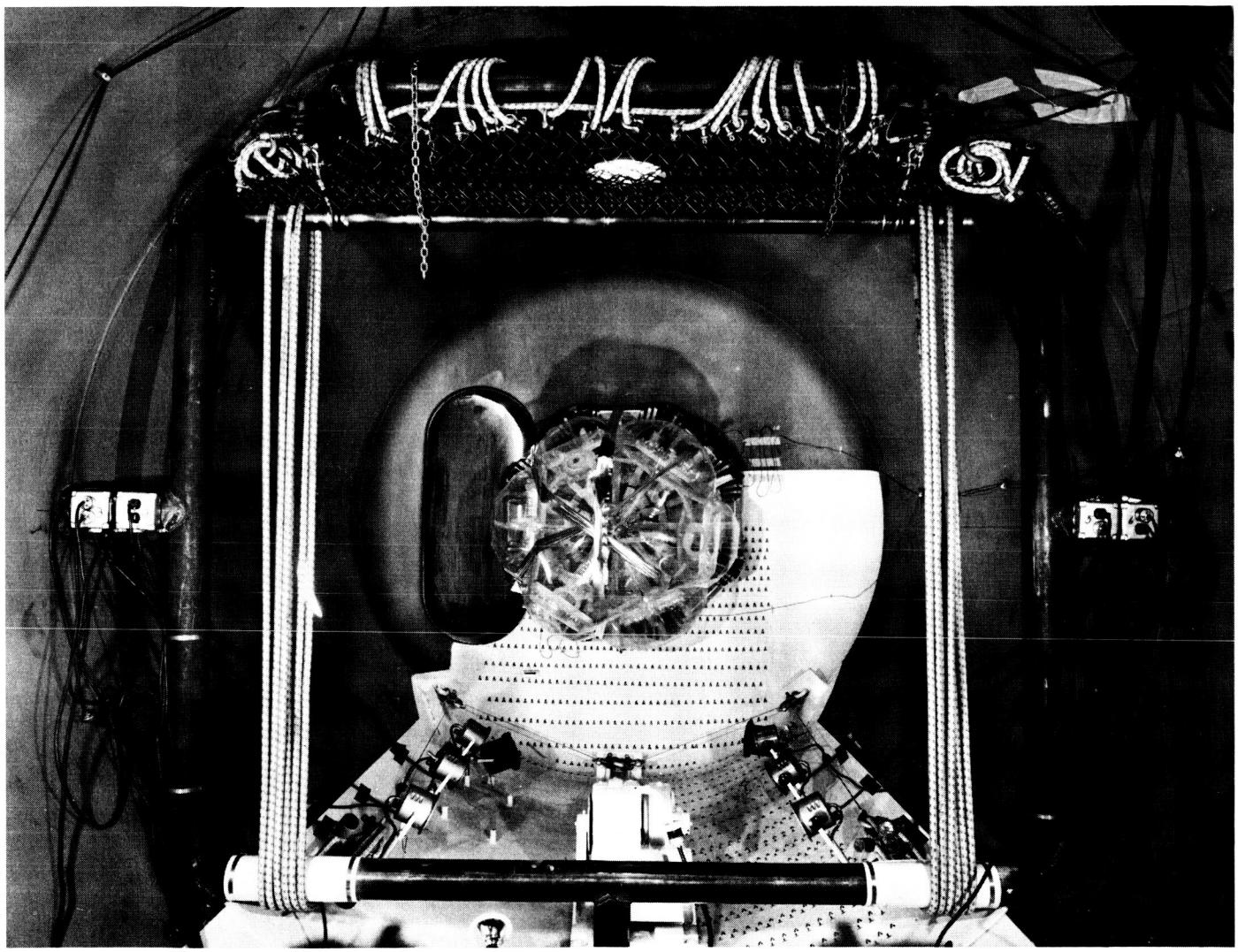

Fig. 13. Test tank interior with limiter in launcher

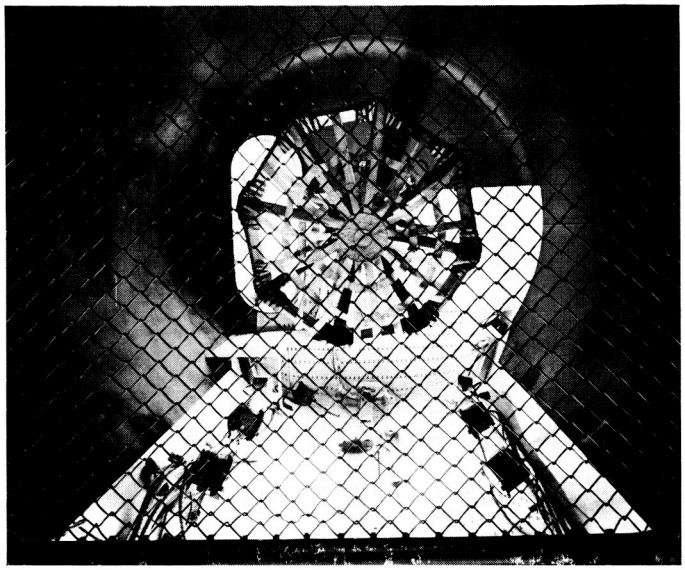

Fig. 14. Launcher extended and catch screen down

Fig. 15. Impact limiter during 100-ft/sec launch

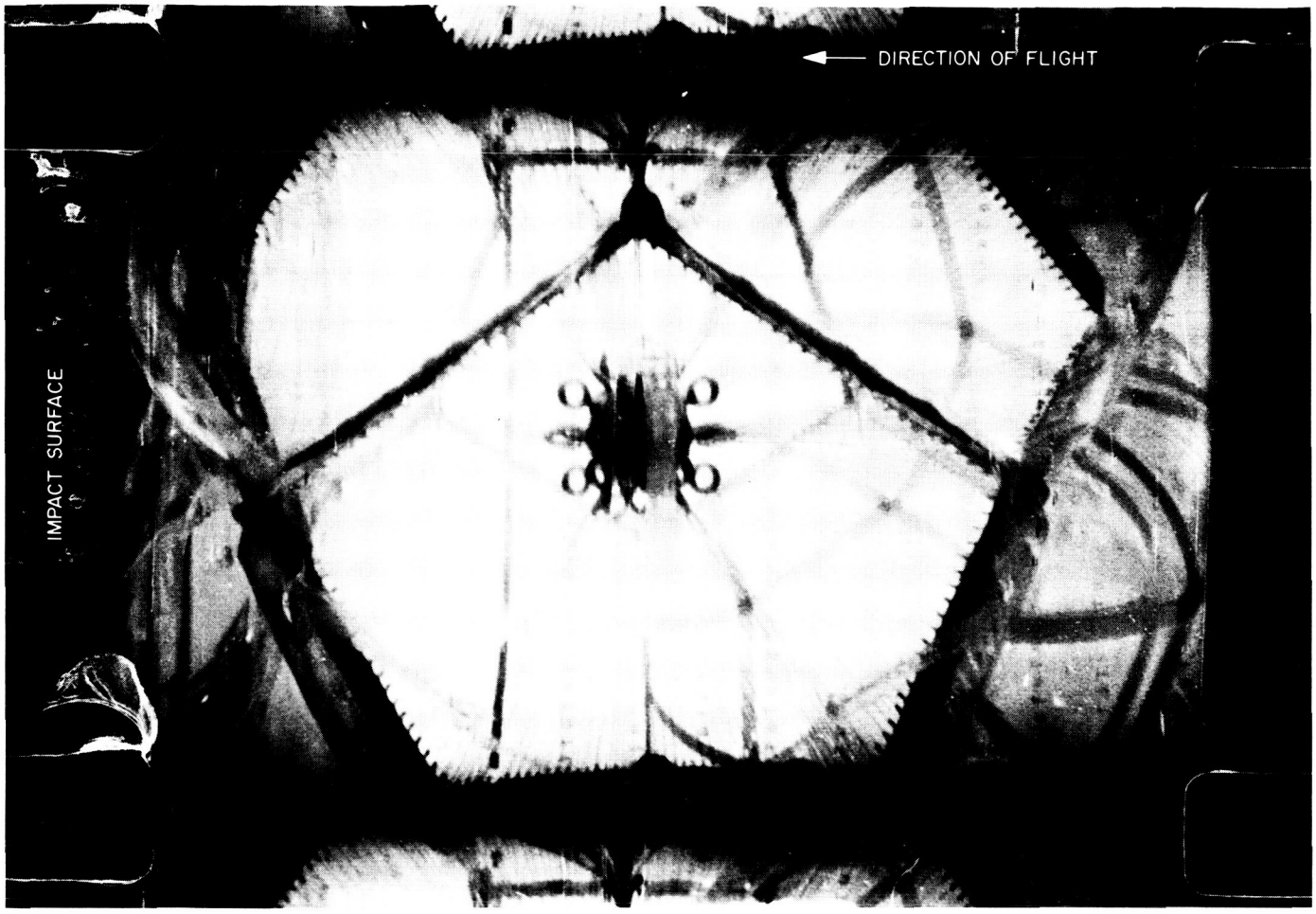

Fig. 16. Impact limiter contacting target, 100-ft/sec

the payload to a near standstill as it approached the impact surface; however, just as the limiter was reaching maximum deflection one of the previously weakened webs began to fail, which allowed the payload to shift toward, and lightly contact, the impact surface. As the impact limiter began to rebound from the impact surface the web failures continued to propagate. This propagation initiated severe skin ruptures and rendered the limiter totally irreparable. Ignoring the limiter failure during rebound, it is felt that the design was validated to an impact velocity of 165 ft/sec during this test. A new prototype was not built to validate the limiter to its design value of 200 ft/sec; however, the static test data indicate that the 200-ft/sec impact can be withstood by an undamaged limiter of the prototype design. Accepting the prototype design as operable at 200 ft/sec and ratioing its payload weight of 12.22 lb to its total weight of 19.08 lb, the conclusion is that at least a 64% payload percentage is achievable in a real design. The authors can see obvious weight penalties in the design which, if removed, would raise the 200-ft/sec payload percentage to 74%. Further improvements beyond this value are certainly feasible in a refined design having a large number of domes.

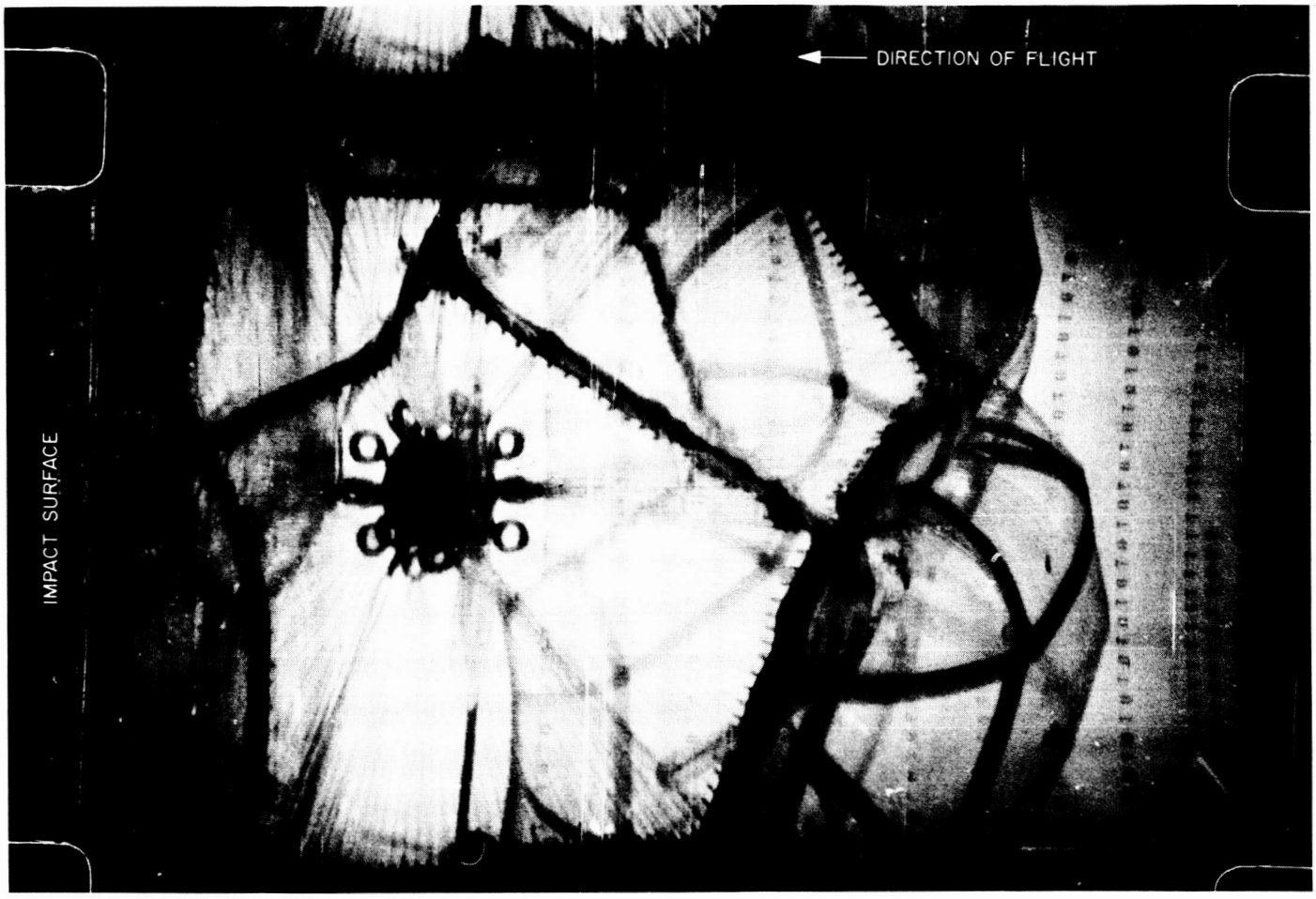

Fig. 17. Impact limiter fully deflected, 100-ft/sec

V. SUMMARY

The design parameters necessary to the sizing of a spherical pneumatic impact limiter are set forth in Section II of this Report. The parameters are frozen into a prototype design which is highlighted in Section III, and the prototype design is validated in testing described in Section IV. The testing, though not completely thorough, builds a very high confidence that the analysis and design are sound, and indicates that payload percentages greater than 74 are feasible for impact velocities of 200 ft/sec. A short film showing the prototype limiter impact tests and showing the limiter test facility is available on loan to those interested by contacting W. E. Layman at the Jet Propulsion Laboratory, 4800 Oak Grove Drive, Pasadena, California.

APPENDIX

Derivations

I. DERIVATION NO. 1

Given: A spherical limiter during impact upon a hard surface which applies reaction force F to the limiter as it decelerates, Sketch No. 1. The limiter of mass m has an instantaneous cg velocity v and instantaneous cg displacement x.

Find: The instantaneous kinetic energy loss of the limiter as a function of the reaction force and decelerating distance. From Newton:

$$F = m\frac{dv}{dt} = m\frac{dv}{dx}\frac{dx}{dt} = mv\frac{dv}{dx} ,$$

$$\therefore \int_0^x F\,dx = \int_{v_0}^{v} mv\,dv$$

$$\therefore \int_0^x F\,dx = \frac{1}{2}mv^2 - \frac{1}{2}mv_0^2 = \text{kinetic energy loss}$$

$$\therefore \quad \boxed{\text{kinetic energy loss} = \int_0^x F\,dx}$$

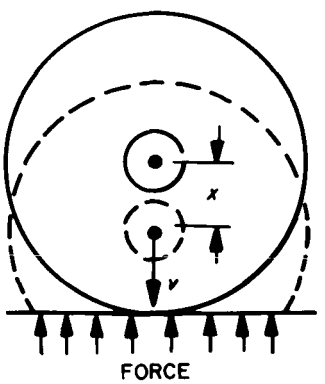

Sketch No. 1

Since the mass of the payload >> mass skin, the cg is approximately coincident with payload.

$$\therefore x \approx \text{payload displacement}^8$$

[8] In the very high impact velocity performance regime of 200 to 500 ft/sec, this approximation becomes less valid and is unconservative because the balloon skin weight becomes a large fraction of the total impacting weight.

II. DERIVATION NO. 2

Given: A spherical limiter of radius R, net internal pressure P, and constructed with N equally-spaced radial cords. During impact a flat section of radius b subtends a half angle Θ, Sketch No. 2.

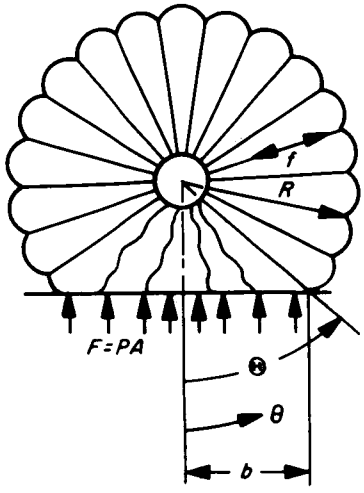

Sketch No. 2

Required: Calculate the force f in each cord as a function of Θ if the mass of the limiter is negligible with respect to the payload.

From inspection, the resultant force F acting on the system is PA (neglecting gravity). But

$$A = \pi b^2 \quad , \quad b = R \sin \Theta$$

$$\therefore F = P\pi R^2 \sin^2 \Theta$$

If the net decelerating force on the payload is defined as F_p and it is assumed that the force f in each cord is the same, then:

$$F_p = \sum_{n=1}^{N} (-f_n \cos \theta_n) = \int \left(\frac{\text{force}}{\text{line}}\right)\left(\frac{\text{lines}}{\text{area}^{9}}\right) dA$$

$$= \int_{\Theta}^{\pi} (-f \cos \theta)\left(\frac{N}{4\pi R^2}\right)(2\pi R^2 \sin \theta \, d\theta)$$

$$= -\frac{fN}{2}\int_{\Theta}^{\pi} \sin \theta \cos \theta \, d\theta = \frac{fN}{4} \sin^2 \Theta$$

But

$$F_p \approx F \quad , \quad \therefore P\pi R^2 \sin^2 \Theta \approx \frac{fN}{4} \sin^2 \Theta$$

$$\therefore \quad \boxed{f \approx \frac{4\pi R^2 P}{N}}$$

[9] Area, in the equation, is the unimpacted surface area of the limiter.

III. DERIVATION NO. 3

Given: A spherical impact limiter of radius R made up of a number of convexities which subtend a half angle α. The perimeter p of each convexity is fastened to the payload by radial cords of length R. The internal pressure P against the effective area A of each convexity creates a force $\mathcal{G}$ per unit length of the convexity's perimeter and a total resultant force $\mathcal{G}_R$ per unit length of loading web, Sketch No. 3.

Find: The convexity intersection γ such that the total radial force applied to the payload is equal to $4\pi R^2 P$.

Consider the topmost convexity:

$$\Sigma \text{ vertical forces} = \overset{\approx 0}{ma} = 0$$

$$\therefore PA = \mathcal{G}\,[\cos(\gamma - \alpha)]\, p$$

where: $\mathcal{G}$ = force/perimeter length

p = perimeter

A = projected area

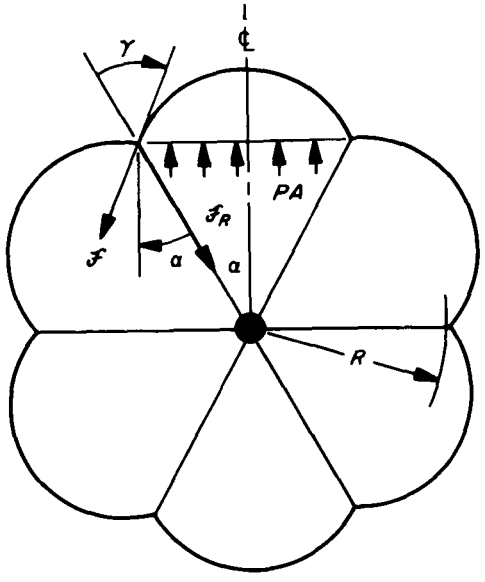

Sketch No. 3

If the forces in the radial direction are summed at the cord intersection, then:

$$\mathcal{G}_R = 2\,\mathcal{G}\cos\gamma = \text{force/web length}$$

Combining the above two equations:

$$\mathcal{G}_R = \frac{2\,PA\cos\gamma}{p\cos(\gamma-\alpha)}$$

and

$$\text{total force} = (\text{force/web length})\,(\text{total web length})$$

But

$$\text{force/web length} = \mathcal{G}_R$$

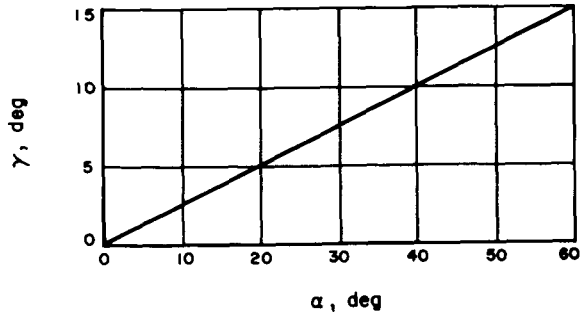

Fig. A-1. Convexity intersection angle vs α

and

$$\text{web length} = \frac{(\text{number of convexities})\,(\text{perimeter})}{2}$$

But

$$\text{number of convexities} = \frac{2}{1-\cos\alpha}\ \text{(Derivation No. 9)}$$

$$\therefore \text{Web length} = \frac{p}{1-\cos\alpha}$$

$$\therefore \text{total force} = \frac{2\,PA\cos\gamma}{(1-\cos\alpha)\,[\cos(\gamma-\alpha)]}$$

But

$$A \approx \pi R^2 \sin^2\alpha$$

$$\therefore \text{total force} = \frac{2\pi R^2\,P\cos\gamma\sin^2\alpha}{(1-\cos\alpha)\,[\cos(\gamma-\alpha)]}$$

$$\equiv 4\pi R^2\,P\ \text{(for solution)}$$

Thus

$$4\pi R^2\,P = \frac{2\pi R^2\,P\cos\gamma\sin^2\alpha}{(1-\cos\alpha)\,[\cos(\gamma-\alpha)]}$$

$$\frac{\sin^2\alpha}{2(1-\cos\alpha)}\cos\gamma = \cos(\gamma-\alpha) = \cos\gamma\cos\alpha + \sin\gamma\sin\alpha$$

$$\therefore \left[\frac{\sin^2\alpha}{2(1-\cos\alpha)} - \cos\alpha\right]\cos\gamma = \sin\alpha\sin\gamma$$

$$\therefore \tan\gamma = \left[\frac{\sin^2\alpha}{2(1-\cos\alpha)} - \cos\alpha\right] / \sin\alpha$$

$$= \frac{\sin^2\alpha - 2\cos\alpha + 2\cos^2\alpha}{2(1-\cos\alpha)\sin\alpha}$$

$$= \frac{(1-\cos\alpha)^2}{2(1-\cos\alpha)\sin\alpha} = \frac{1-\cos\alpha}{2\sin\alpha}$$

$$\therefore \boxed{\gamma = \tan^{-1}\left(\frac{1-\cos\alpha}{2\sin\alpha}\right)} \qquad \boxed{\gamma \approx \frac{\alpha}{4}}$$

From Fig. A-1

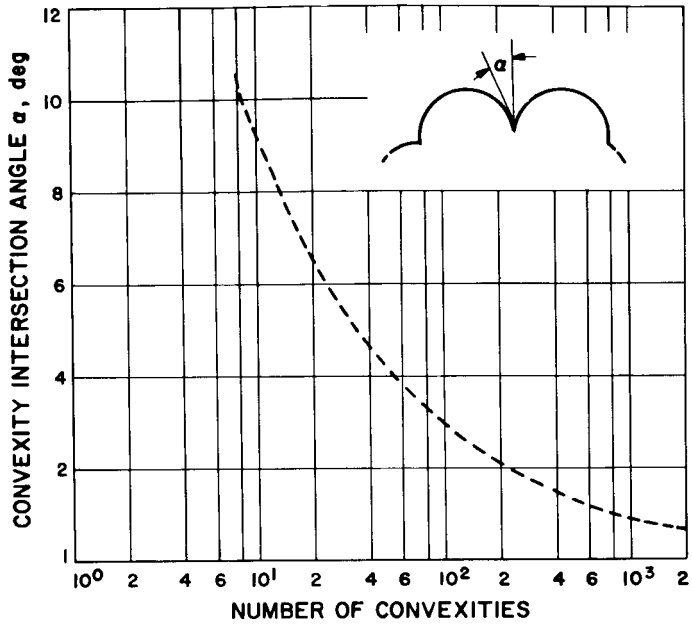

Fig. A-2. Convexity intersection angle vs number of convexities

IV. DERIVATION NO. 4

Given: A membrane in the form of a surface of revolution with net internal pressure P, and thickness t, Sketches No. 4 and 5.

Find: Criterion for stability of the shape.

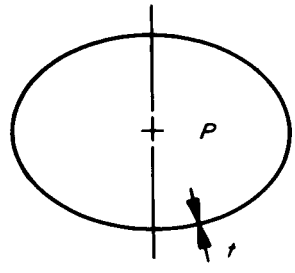

Sketch No. 4

Consider the section as shown in Sketch No. 5. For equilibrium the force exerted by the gas PA must equal the downward force component of the restraining hoop stresses σ_1 which produce tension force $\mathcal{F}$ per unit length around the perimeter, i.e.,

$$PA = 2\pi r_1 \mathcal{F} \sin\theta$$

But

$$\mathcal{F} = \frac{\text{stress} \times \text{area}}{\text{length}} = \frac{2\pi r_1 t \sigma_1}{2\pi r_1} = \sigma_1 t$$

Also

$$A = \pi r_1^2$$

$$\therefore \pi r_1^2 P = 2\pi r_1 t \sigma_1 \sin\theta$$

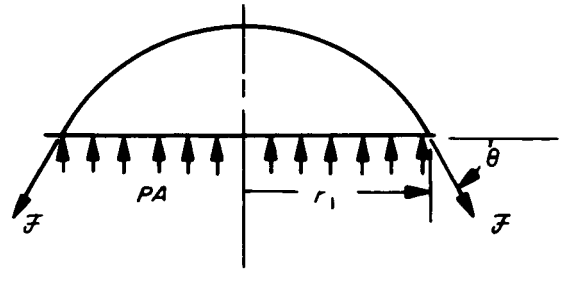

Sketch No. 5

Thus

$$\sigma_1 = \frac{Pr_1}{2t\sin\theta}$$

Next consider a small element of membrane as shown in Sketch No. 6. For equilibrium the components of the hoop stresses in the direction of the pressure force must equal the pressure force.

Sketch No. 6

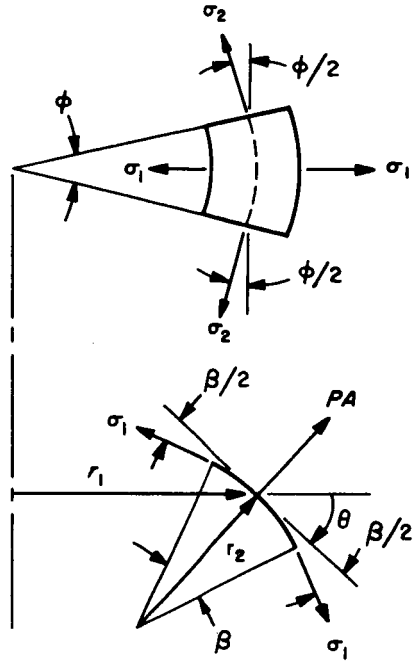

$$\therefore PA = 2\sigma_1 t r_1 \phi \sin\frac{\beta}{2} + 2\sigma_2 t r_2 \beta \sin(\phi/2)\sin\theta$$

But

$$A = r_1 \phi r_2 \beta \quad , \quad \sin\frac{\beta}{2} \approx \frac{\beta}{2} \quad , \quad \sin(\phi/2) \approx \frac{\phi}{2}$$

$$\therefore Pr_1 \phi r_2 \beta = \sigma_1 t r_1 \phi \beta + \sigma_2 t r_2 \beta \phi \sin\theta$$

$$\therefore \quad \sigma_2 = \left(\frac{Pr_1}{t} - \sigma_1 \frac{r_1}{r_2}\right)/\sin\theta$$

But

$$\sigma_1 = \frac{Pr_1}{2t\sin\theta}$$

$$\therefore \quad \boxed{\sigma_2 = \frac{Pr_1}{t\sin\theta}\left(1 - \frac{r_1}{2r_2\sin\theta}\right)}$$

But for stability

$$\sigma_2 \geqq 0$$

$\therefore$ the stability criterion is:

$$1 - \frac{r_1}{2r_2\sin\theta} \geqq 0$$

$$\therefore \quad \boxed{r_2 \geqq \frac{r_1}{2\sin\theta}}$$

If

$$r_2 = \frac{r_1}{2\sin\theta}$$

then

$$\sigma_2 = 0$$

and

$$\sigma_1 = \frac{Pr_2}{t}$$

This limiting stable configuration is shown in Sketch No. 7.

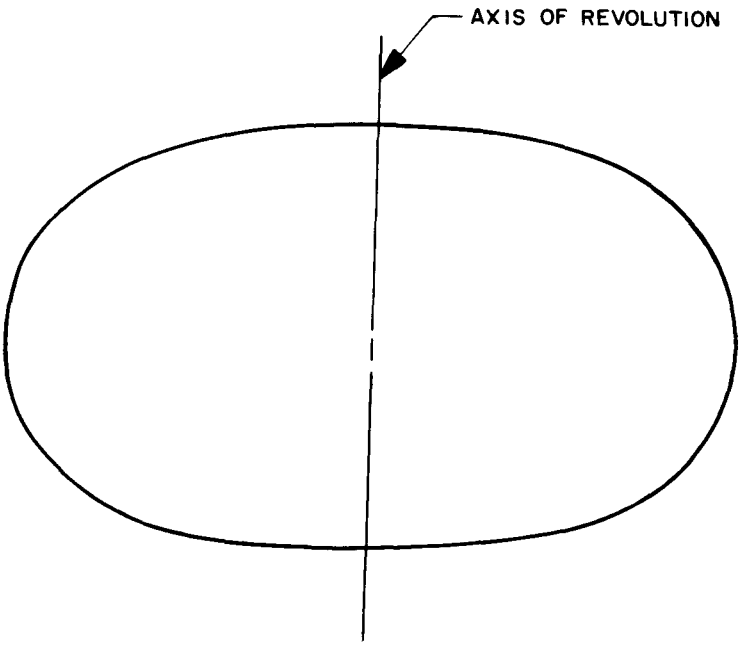

Sketch No. 7

V. DERIVATION NO. 5

Given: An impact limiter skin made up of numerous spherical convexities all tangent to one another at a radius R from the limiter center, Sketch No. 8.

Find: The total surface area of the limiter as a function of the half angle α.

$$\text{Surface area} = \text{Number of convexities} \times \text{area of convexity} = \eta A$$

But

$$\eta \approx \frac{2}{1-\cos\alpha} \text{ (Derivation No. 9)}$$

and

$$A = 2\pi r^2 (1+\sin\alpha) = 2\pi R^2 \tan^2\alpha\,(1+\sin\alpha)$$

$$\therefore \text{total surface area} \approx 4\pi R^2 \frac{\tan^2\alpha\,(1+\sin\alpha)}{1-\cos\alpha}$$

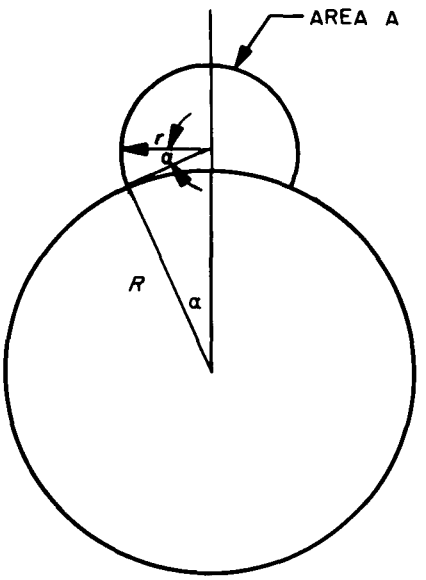

Sketch No. 8

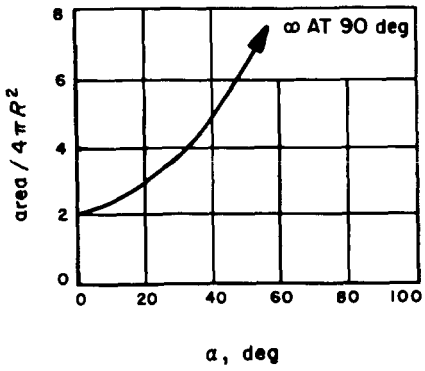

Fig. A-3. Convexity area vs α

VI. DERIVATION NO. 6

Given: An impact limiter skin made up of numerous spherical convexities all tangent to one another at a radius R from the limiter center, Sketch No. 9.

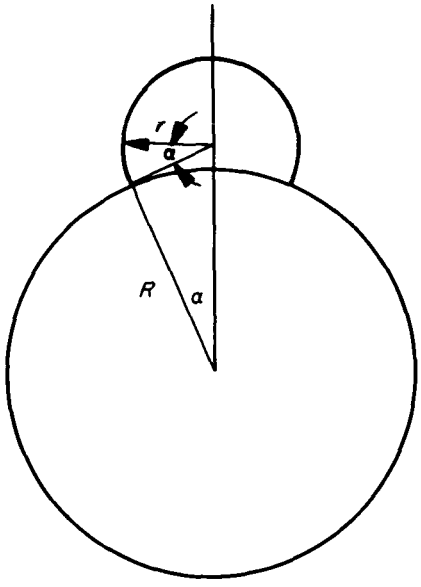

Sketch No. 9

Find: The total[10] skin weight of the limiter as a function of the half angle α.

Skin weight = density × thickness × area

But

$$\text{density} = \rho$$

$$\text{thickness} = t = \frac{Pr}{2\sigma} = \frac{PR\tan\alpha}{2\sigma}$$

(σ: skin's working stress)

$$\text{area} = 4\pi R^2 \tan^2\alpha \frac{(1+\sin\alpha)}{(1-\cos\alpha)}$$

$$\therefore \boxed{\text{skin weight} = \frac{2\pi R^3 \rho P}{\sigma} \tan^3\alpha \frac{(1+\sin\alpha)}{(1-\cos\alpha)}}$$

[10] See Fig. 5 in Section II of Report for a plot of skin-weight parameter vs number of convexities.

VII. DERIVATION NO. 7

Given: An impact limiter made up of numerous spherical convexities all tangent to one another at a radius R from the limiter center, Sketch No. 10.

Find: The total[11] volume of the limiter as a function of the half angle α.

$$\text{Total volume} = \frac{4}{3}\pi R^3 + (\text{number of convexities})\,(\text{volume of convexity})$$

But

$$\text{number of convexities} \approx \frac{2}{1-\cos\alpha}\ \text{(Derivation No. 9)}$$

and

$$\text{volume of convexity} = \frac{\pi r^3}{3}\left[2 + \sin\alpha\,(\cos^2\alpha + 2)\right]$$

Also

$$r^3 = R^3 \tan^3\alpha$$

$$\therefore\ \boxed{\text{total volume} \approx \frac{4}{3}\pi R^3 + \frac{2\pi R^3 \tan^3\alpha}{3(1-\cos\alpha)}\left[2 + \sin\alpha\,(\cos^2\alpha + 2)\right]}$$

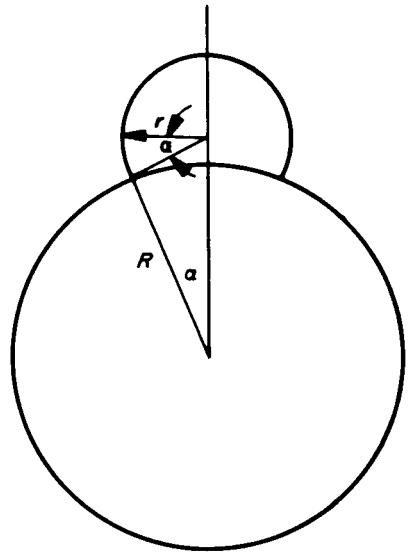

Sketch No. 10

[11] See Fig. 5 in Section II for a plot of balloon volume parameter vs number of convexities.

VIII. DERIVATION NO. 8

Given: An impact limiter skin made up of numerous spherical convexities all tangent to one another at a radius R from the limiter center, Sketch No. 11.

Find: The total length of seams between convexities as a function of the half angle α.

$$\text{Seam length} = \text{number of convexities} \times \frac{1}{2}\,\text{perimeter of convexity}$$

But

$$\text{number of convexities} \approx \frac{2}{1-\cos\alpha}$$

and

$$\text{perimeter} = 2\pi R \sin\alpha$$

$$\text{Seam length} \approx \left(\frac{2}{1-\cos\alpha}\right)(\pi R \sin\alpha) = 2\pi R\left(\frac{\sin\alpha}{1-\cos\alpha}\right)$$

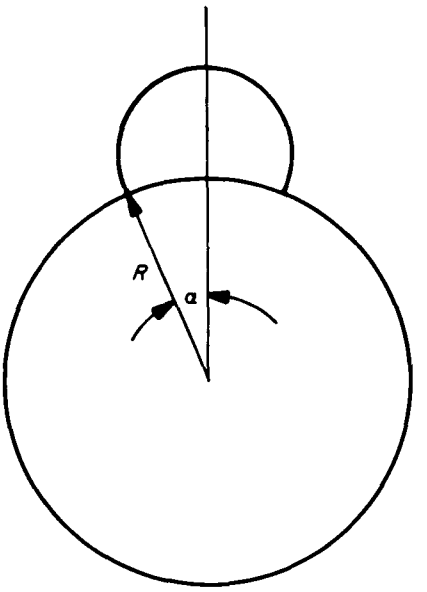

Sketch No. 11

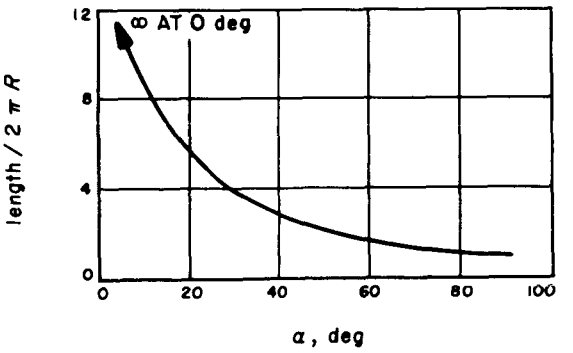

Fig. A-4. Length of loading webs vs α

IX. DERIVATION NO. 9

Given: A spherical skin of radius R.

Find: The number of circular skin sections of radius, $R \sin \alpha$, required to cover the surface of the sphere, Sketch No. 12.

$$\text{Number of sections} \approx \frac{\text{surface area of sphere}}{\text{surface area of section}}$$

But

$$\text{surface area of sphere} = 4\pi R^2$$

and

$$\text{surface area of section} = 2\pi R^2 (1 - \cos \alpha)$$

$$\therefore \text{number of sections} = \frac{4\pi R^2}{2\pi R^2 (1 - \cos \alpha)}$$

$$\therefore \boxed{\text{number of sections} \approx \frac{2}{1 - \cos \alpha}}$$

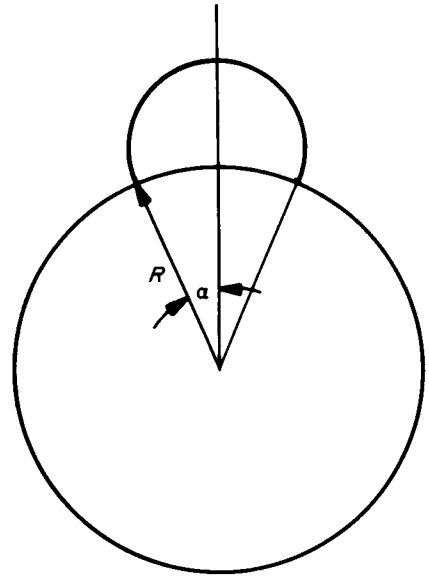

Sketch No. 12

X. DERIVATION NO. 10

Given: A spherical impact limiter with initial volume V_1 filled with a gas of initial pressure P_1 and temperature T_1, Sketch No. 13. The impact limiter is then instantaneously compressed to volume V_2 and the gas compresses to pressure P_2 and temperature T_2. The gas of mass M has gas constant $\mathscr{R}$, ratio of specific heats γ, and specific heat at constant volume C_v.

Find: The total gain in energy of the gas.

Energy gain $= \Delta E = C_v M \Delta T$

But for an isentropic expansion:

$$\frac{T_2}{T_1} = \left(\frac{V_1}{V_2}\right)^{\gamma - 1} \qquad \text{(ideal gas)}$$

Also

$$M = \frac{P_1 V_1}{\mathscr{R} T_1} \quad , \qquad \Delta T = T_2 - T_1 = T_1 \left(\frac{T_2}{T_1} - 1\right)$$

$$\therefore \boxed{\text{energy gain} = \frac{C_v P_1 V_1}{\mathscr{R}} \left[\left(\frac{V_1}{V_2}\right)^{\gamma - 1} - 1\right]}$$

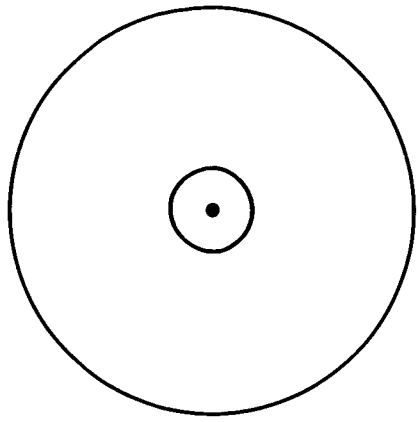

Sketch No. 13

NOMENCLATURE

A	area, ft^2
f	force per cord, lb
F	decelerating force, lb
$\mathcal{G}$	force per unit length of convexity perimeter, lb/ft
m	mass of limiter including payload, (lb sec^2)/ft
M	mass of gas, (lb sec^2)/ft
n	indexing subscript referring to a particular cord
N	number of cords
p	perimeter of convexity, ft
P	net internal pressure, lb/ft^2
r	radius of spherical convexity, ft
$r_{1,2}$	various radii, ft
R	radius of limiter, ft
t	thickness of convexity material, ft
T	temperature of gas, °R
v	velocity of center of gravity of limiter, ft/sec
V	volume of gas, ft^3
x	displacement of cg, ft
α	half angle subtended by convexity, rad
β	various angles, rad
γ	half intersection angle between convexities, rad
η	number of convexities
θ	various angles, rad
Θ	half angle subtended by impact area, rad
ρ	weight density of convexity material, lb/ft^3
σ	skin working stress, lb/ft^2
σ_1, σ_2	principal stresses in convexity, lb/ft^2
ϕ	various angles, rad

ACKNOWLEDGMENT

Special acknowledgements are made to: A. J. Delgadillo, D. E. Huls, R. H. Almaguer, R. W. Clark, H. Gold, F. J. Cook, W. C. Schaefer, D. D. Lo Giurato, D. R. Maxeiner, R. L. Hansen, J. R. Kallen, and E. A. Otto, without whom this project could not have been successfully completed.